

## Numerical study of stress distribution in sheared granular material in two dimensions

S. G. Bardenhagen\* and J. U. Brackbill

*Los Alamos National Laboratory, Los Alamos, New Mexico 87545*

D. Sulsky

*University of New Mexico, Albuquerque, New Mexico 87131*

(Received 22 March 2000)

We simulate the response of dense granular material to shear. Our simulations use a micromechanical model which includes realistic material models for each deformable grain, and a Coulomb friction model for interactions between grains. We measure the probability density function (PDF) governing the volume distribution of stress for monodisperse and polydisperse samples, circular and polygonal grains, and various values of microscopic friction coefficients, yield stresses, and packing fractions. Remarkably, PDF's are similar in form for all cases simulated, and similar to those observed in experiments with granular materials under both compression and shear. Namely, the simulations yield an exponential probability of large stresses above the mean. The relationship between distributions of boundary tractions and volume distributions of stress is discussed. The ratio of normal and tangential components of traction on the boundary defines a bulk frictional response, which is shown to increase with the intergranular friction coefficient. However, the bulk friction is always larger than the intergranular friction for densely packed samples. Bulk friction is also strongly dependent on grain size distribution and shape. New observations of force-chain banding during recrystallization, of slip systems in monodisperse samples, and of the effects of plastic yield, are also presented.

PACS number(s): 45.70.-n, 83.70.Fn, 62.20.-x, 46.25.Cc

### I. INTRODUCTION

The physics of granular material is complex. At times, it can display behavior reminiscent of solids, fluids, or gases, but at others it can behave differently from any of these forms of matter [1,2]. Further, the absence of a continuous displacement field in a granular material is an obstacle to characterizing the response of granular materials by relating stress and strain as is usually done in continuum mechanics [3]. Through micromechanical simulations, like those presented here, one seeks to discover the underlying physical laws governing the behavior of granular materials, and to use these to develop macroscopic models that will reproduce some of the observed complexity.

Simple models of the interactions among individual grains have provided remarkable agreement with experiments. For example, the  $q$  model [4] predicts the distribution of boundary forces associated with force chains [5,6], and contact dynamics simulations explore the relationship between Coulomb friction between grains and the bulk behavior [7,8]. These models idealize the material properties of individual grains and of their interactions, and thus leave unanswered many questions about the bulk properties of real granular material. Major questions remain unresolved, such as the choice of appropriate variables for a bulk description, whether hydrodynamic equations are applicable, and how to include history dependence [9].

With careful attention to efficient algorithms, micromechanical simulations can be used effectively to study the physics of granular materials. For individual grains, realistic

constitutive models are available. With the addition of a contact model for the interactions between grains, one can simulate many grains in a single computational experiment [10,11].

A striking result of experiments and simulations of granular materials is the high level of fluctuations that occur when samples undergo shear or compression. Under compression, a small fraction of the grains participate in force chains and have large contact forces. Force chains seem to be associated with an exponential probability distribution of forces and stresses above the mean [12–14]. A simple theoretical model for the probability distribution of the magnitude of normal contact forces [4] assumes that inhomogeneous particle arrangements cause an unequal distribution of force transmission between neighboring particles, which leads to chains of particles transmitting above average forces.

The simulation of granular materials under shear is well suited to the study of the statistics of the observed fluctuations. Under compression, the network of force chains is stationary in time over a range of deformation. If the range of deformation is increased, damage to the sample will result. To identify the probability density function from simulation experiments of compressive loading, it is necessary either to perform a single simulation with a very large number of grains, or to perform a very large number of simulations with a moderate number of grains. Under shear [15,16], force chains persist briefly before being replaced. Slow shear generates an ensemble of statistically independent states near static equilibrium with similar history [17]. Intermittently, the grains bind and deform, i.e., translation and sliding are insufficient to accommodate the deformation. Further shear relieves binding and the force chains disappear to be replaced by new force chains. Thus, simulations with a relatively small number of grains subjected to large strains pass

---

\*On leave. Present address: Dept. of Mechanical Engineering, University of Utah, Salt Lake City, UT 84112.

through a large number of statistically independent states, from which one can recover the underlying probability density function.

Although there are several recent modeling studies of granular shear using the distinct element method [18–20], the statistics of the fluctuations are not reported. Morgan [20] considers the effect of particle size distribution and friction on the strength of granular shear zones. Schwarz *et al.* [18] examine strain rate dependence and strain distribution under shear. The cases considered by Schwarz *et al.* are for lower strain rates than are considered here, but with similar fill densities. Morgan and Boettcher [19], using a contact law derived from Hertz-Mindlin contact theory, observe stress bridging that migrates through the shear zone with increasing strain. Schwarz *et al.* [18], using a repulsive core potential between elements, do not observe stress bridging.

Here, the volume and boundary distribution of stress are examined for dense granular material under continuous shear. Results of simulations with deformable, elastic-plastic grains and Coulomb friction are presented for monodisperse and polydisperse granular samples, circular and polygonal cross-section grains, and various values of the intergranular friction, packing fraction, and yield stress. Observations on the effects of these parameters on resistance to shear, load carrying mechanisms, and deformation modes are made.

## II. APPROACH

In experiments that shear disks at constant volume, a transition occurs at a critical packing fraction  $\gamma \approx 0.78$  [16]. The packing fraction is defined as the ratio of the volume of the grains to that of their container. Below the transition, force chains appear occasionally. Contact is brief and well modeled as collisions using, for example, the discrete element method. Above the transition, grains are in persistent contact, and a dense, evolving network of force chains is continually present. At the transition and above, the regime primarily of interest here (referred to as “dense” granular material), persistent contact and large, localized stress require accurate modeling of contact tractions and granular deformation.

We simulate granular materials with the material-point method (MPM) [21–23]. The simulations are two dimensional. Grains deform according to a continuum mechanical model in which conservation of mass and momentum are enforced. If  $\rho(\mathbf{x}, t)$  is the mass density at point  $\mathbf{x}$  at time  $t$ , and  $\mathbf{v}(\mathbf{x}, t)$  is the velocity field, then conservation of mass is

$$\frac{d\rho}{dt} = -\rho \nabla \cdot \mathbf{v}, \quad (1)$$

in which the time derivative is the material derivative

$$\frac{d}{dt} = \frac{\partial}{\partial t} + \mathbf{v} \cdot \nabla. \quad (2)$$

Conservation of momentum is

$$\rho \frac{d\mathbf{v}}{dt} = \nabla \cdot \boldsymbol{\sigma}, \quad (3)$$

where  $\boldsymbol{\sigma}$  is the Cauchy stress tensor. Different materials are modeled through a constitutive equation that relates stress to

strain or strain rate. Versions of hyperelasticity, hypoelasticity, plasticity, and viscoelasticity have been implemented.

In the discrete formulation, each grain consists of a finite collection of material points that are tracked throughout the simulation. Each material point is given an initial mass consistent with the material density and volume of the point. Material parameters such as Young’s modulus, Poisson’s ratio, and yield strength are also assigned to each material point according to the material it represents. As the numerical solution proceeds, the material points are updated and carry the solution variables such as velocity, stress, and strain. (By contrast, in the distinct element method contact forces between grains are the principal variables, and the volume distribution of stress is unknown [24,25].) Finite deformation constitutive models with internal variables are easily implemented in MPM, and accurately applied, because of error-free advection of constitutive parameters.

To determine the motion of the material points in an efficient manner, information from the material points is projected onto a background computational grid. The continuum equations are discretized on this grid using standard finite differences or finite elements. The solution on the grid is then used to update the position and velocity of the material points. Also, strain increments computed on the grid are interpolated to the material point position so that a constitutive equation can be evaluated for each material point to update its stress state. Details may be found in the references. The material-point method has been validated on such problems as elastic wave propagation [21], the Taylor impact problem [22,23], and the upsetting problem [23]. Simulations with MPM have been compared to the same simulations with other finite element and finite difference methods, and compared to analytical solutions and experiments.

Interactions between grains are modeled by a kinematic contact algorithm, which forbids interpenetration but allows separation, sliding with friction, and rolling [11]. Calculation of a Coulomb friction law in a common rest frame eliminates a separate contact detection step, achieves a solution with one sweep through the computational mesh, and yields a linear scaling of the computational cost with the number of grains [11]. By comparison, pairwise interaction algorithms scale quadratically. It is also worth noting that the complexity of the contact algorithm does not increase if the grain shape is varied, so one can easily model complex initial geometry and grain deformation. Momentum and energy transport during collisions have been investigated with good results [26], and other tests show reasonable accuracy for contact forces [11] using MPM.

In this paper, grains are modeled using von Mises plasticity with linear hardening. A plastic material model dictates a linear elastic material response until a yield criterion is reached. The von Mises yield criterion is  $3J_2 - Y^2 = 0$ , where  $\mathbf{s}$  is the deviatoric stress tensor,  $\mathbf{s} = \boldsymbol{\sigma} - \text{Tr}[\boldsymbol{\sigma}]/3$ ,  $J_2$  is the second invariant of  $\mathbf{s}$ ,  $J_2 = \frac{1}{2}\mathbf{s}:\mathbf{s}$ , and  $Y$  is the plastic yield stress. Linear hardening means that  $Y$  increases linearly with the second invariant of the plastic strain tensor. The material constants are chosen to model the energetic crystal HMX (high melting explosive, a mixture of cyclotetramethylene, tetranitramine, and octogen). The shear and bulk moduli are 7.5 GPa and 11.4 GPa, the initial yield strength is 300 MPa, the hardening modulus is 10 MPa, and the density is 1900

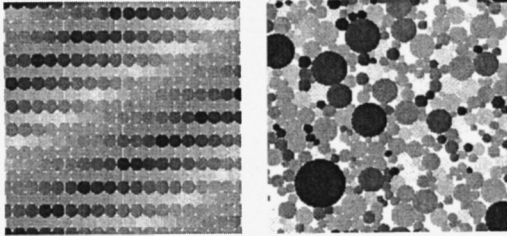


FIG. 1. Monodisperse and polydisperse granular material. Grains are distinguished by shading.

$\text{kg/m}^3$ . A nominal friction coefficient of 0.3 is used in the simulations and the effect of varying it is examined. The actual friction coefficient associated with HMX is hard to measure, and may be higher [27].

Ultimately of interest is the accurate numerical simulation of the response of plastic bonded explosives (PBXs), which are very dense,  $\gamma > 0.90$ , particulate composites, with grains that are embedded in a polymeric binder. For these materials shear is accommodated in part by granular fracture [28]. For large shear, debonding of the interstitial material from the grains also plays a role. In the interest of starting with a more tractable problem and comparing with experimental data on the microscale (essentially only available post-mortem for PBXs), we consider dry granular material with lower packing fractions,  $\gamma = 0.65$  and  $0.78$ , where fracture is unlikely. The effects of grain size distribution, material properties, and friction coefficient are studied.

We consider both monodisperse and polydisperse samples of granular material. For the monodisperse samples, we begin with a regular hexagonal packing of 370, same radius cylinders, Fig. 1. The maximum packing fraction for a hexagonal array in two dimensions is  $\pi/2\sqrt{3} \approx 0.91$ . A  $5.1 \mu\text{m}$  gap between  $32.6 \mu\text{m}$  radius cylinders reduces the packing fraction to  $\gamma = 0.78$ . Reducing the cylinder radius further to  $29.7 \mu\text{m}$  results in  $\gamma = 0.65$ . A  $1.26 \times 1.22 \text{ mm}$  domain is resolved by a  $156 \times 150$  uniform grid with square cells  $8.12 \mu\text{m}$  on a side, which yields approximately 50 cells per cylinder for  $\gamma = 0.78$ . There are roughly four material points per cell.

For the polydisperse case, we consider an “equivalent” geometry with the same packing fraction, same average grain area, and 369 cylinders, Fig. 1. The cylinder radii range from  $15.6$  to  $125 \mu\text{m}$ , with an average of  $28.7 \mu\text{m}$ . The size distribution is chosen to approximate that found in a particular PBX [26]. [In the real material the packing fraction is  $\gamma = 0.93$  on account of many very small ( $< 1 \mu\text{m}$ ) grains.] The  $1.2 \text{ mm}$  square domain is resolved comparably to the monodisperse case by a  $150 \times 150$  grid, which results in a cell size of  $8.06 \mu\text{m}$ .

To induce shear, grains are attached to the left and right boundaries, and the right boundary is moved upward to give an average shear strain rate of  $8 \times 10^4/\text{s}$ . Periodicity is imposed in the vertical direction. The monodisperse and polydisperse samples are subjected to average shear strains in excess of 300%.

### III. RESULTS

#### A. Shearing of monodisperse granular material

First we examine the response of the dense,  $\gamma = 0.78$ , monodisperse sample. When grains are in persistent contact,

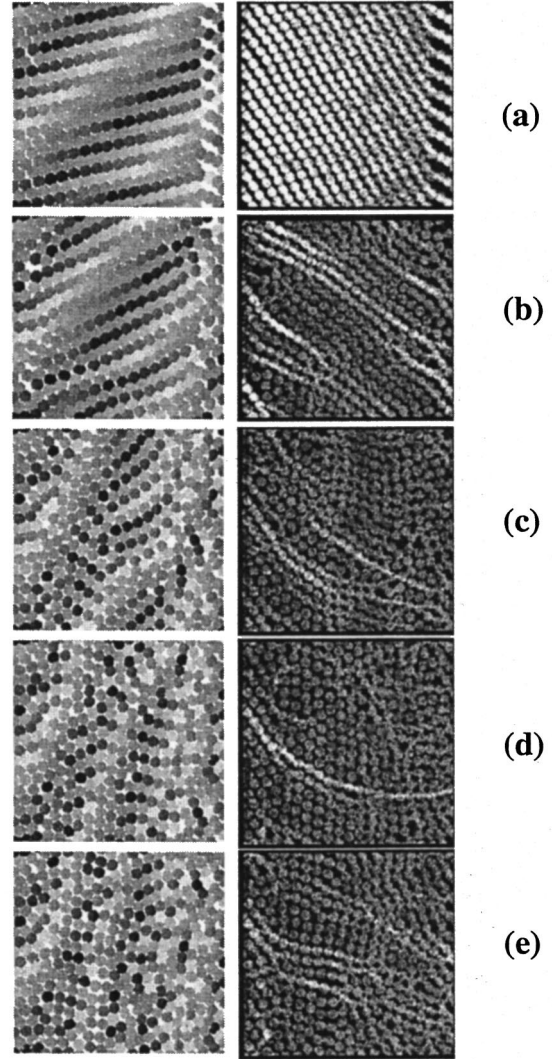


FIG. 2. Sheared states of the monodisperse sample,  $\gamma = 0.78$ . Left, grains are distinguished by shading; right, high stress force chains are indicated by light tones for five average shear states (a) 29%, (b) 70%, (c) 139%, (d) 213%, and (e) 284%.

shear is accommodated by sliding and rolling. This causes local dilation and decreases the packing order, first near the left and right boundaries, Fig. 2. By approximately 150% shear, some disorder and dilation is visible in the center. However, significant order is visible at all times as clumps of particles reorder into regular hexagonal packings locally, or “recrystallize” [17].

The difference in principal stress is detected optically for photoelastic materials [5,6,12,14,16]. To compare with experiments, we display the spatial variation of the difference in principal stresses in Fig. 2. In Cartesian coordinates, the stress tensor at any spatial point has the form

$$\boldsymbol{\sigma} = \begin{bmatrix} \sigma_{11} & \sigma_{12} & \\ \sigma_{12} & \sigma_{22} & \\ & & \sigma_{33} \end{bmatrix}, \quad (4)$$

where the 3 direction is perpendicular to the shearing plane. Although no out-of-plane shear can develop during plane

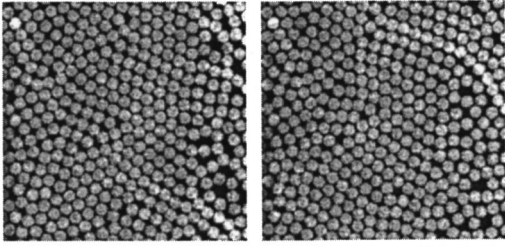


FIG. 3. For the lower density, monodisperse case,  $\gamma=0.65$ , dilation occurs near the right boundary. Stress force chains, which are indicated by light tones, are less evident than for the higher density case. Average shears are 146% (left) and 167% (right).

strain deformation of an isotropic material, the out-of-plane stress  $\sigma_{33}$  is generally nonzero. For this presentation it is convenient to work with the diagonalized stress tensor, which can be written

$$\boldsymbol{\sigma} = \begin{bmatrix} \bar{\sigma} + \Delta\sigma/2 & & \\ & \bar{\sigma} - \Delta\sigma/2 & \\ & & \sigma_3 \end{bmatrix}, \quad (5)$$

where  $\bar{\sigma} = (\sigma_1 + \sigma_2)/2$ ,  $\Delta\sigma$  is the (in-plane) principal stress difference, and the principal stresses are denoted by  $\sigma_i$ .

Contour plots of difference in principal stress reveal force chains involving many grains. Figure 2 shows force chains for  $\gamma=0.78$  and Fig. 3 for  $\gamma=0.65$ . The plots are individual time slices from the data sets used in Fig. 4. The force chain plots are made by contouring as white all values greater than 1.9 times the mean. The threshold values are 216 MPa for  $\gamma=0.78$  and 162 MPa for  $\gamma=0.65$ , and are indicative of the magnitudes of the force chain stresses.

The chain networks evolve from a regular pattern in the initial hexagonal array, Fig. 2 (a). As rows buckle, disorder propagates inward. Even though the middle is still regularly packed, Figs. 2(b) and 2(c), the force chain density is substantially reduced. The remaining order causes force chain banding, i.e., several adjacent force chains develop as primary load paths simultaneously and the volume-averaged stress increases. Even after the order of the packing is lost overall, the force chains look similar, Figs. 2(d) and 2(e). For the largest shear, Fig. 2(e), some order is reestablished and force chain banding recurs. (In a recent simulation of the shear of a dense monodisperse granular material with the discrete element method, in which grains are modeled as

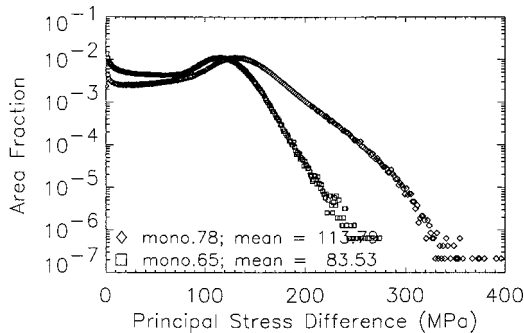


FIG. 4. Principal stress difference distributions for  $\gamma=0.65$  and  $\gamma=0.78$  monodisperse granular material.

points interacting through potentials, persistent contact is not observed, force chains are dispersive, and banding is not apparent [18].)

For the lower density sample,  $\gamma=0.65$ , deformation is accommodated differently. Following the initial compaction, which is similar to Fig. 2(a), a dilated zone develops near the right (shearing) boundary as seen in Fig 3. Grains in the dilated region, or shear band, transfer the shearing stimulus through collisions; persistent contact is not maintained. Force chains only form occasionally, involve only a few grains, and generate lower stresses than the dense case, as is quantified in the discussion of Fig. 4. Force chains are quickly dissipated in the bulk material beyond the shear band, as seen in Fig. 3. Consequently, a weak stimulus reaches the bulk of the grains and substantial shearing ( $\geq 125\%$ ) is required to overcome the inertial resistance of the initially stationary grains.

In Fig. 4 are plotted histograms for both densities of monodisperse material giving the fraction of the total area within which the computed principal stress difference lies within a small interval. The data are comprised of snapshots which give the principal stress difference at every grid point at a sequence of times. The sequence begins after the initial order is disrupted and the shearing deformation is well developed throughout the material. This corresponds to a shear strain above 58% for  $\gamma=0.78$  and a shear strain greater than 125% for  $\gamma=0.65$ . Snapshots are separated by about 2% strain; 8% strain is sufficient for the pattern of force chains to change completely. The data set consists of 133 snapshots for  $\gamma=0.78$  and 101 snapshots for  $\gamma=0.65$ . There are, of course, for any given snapshot, strong spatial correlations. For example, distributions in the right and left half of the sample have the same mean value and variance as in the whole.

For both packing fractions the distribution is exponential above the mean over four decades (although with substantially different exponent multipliers). We note that an exponential distribution of the particle contact forces is inferred from the photoelastic response in a recent experiment on continuously sheared granular material [16]. These distributions, found numerically and experimentally for sheared samples, are reminiscent of exponential distributions established for granular material under compression [4,14]. An exponential probability distribution of the principal stress difference within granular material is surprisingly insensitive to the type of loading and the packing fraction. It appears to be a characteristic of the heterogeneous nature of the load carrying mechanism in granular material.

While both histograms in Fig. 4 show an exponential character over many decades, that for the dense packing fraction appears to have some downward curvature. While the statistics are not quite good enough to make an accurate determination, a more convincing downturn is seen in the histogram of equivalent stress for  $\gamma=0.78$ , Fig. 5. Plastic yielding first occurs when the equivalent stress ( $\sqrt{3}J_2$ ) equals 300 MPa, the initial yield strength. Stress states significantly greater than the initial yield strength are difficult to obtain due to the greatly reduced material stiffness during plastic deformation. The downturn indicates that plastic yielding is rare. Stress is calculated on material points, but average values for computational cells (each containing several material

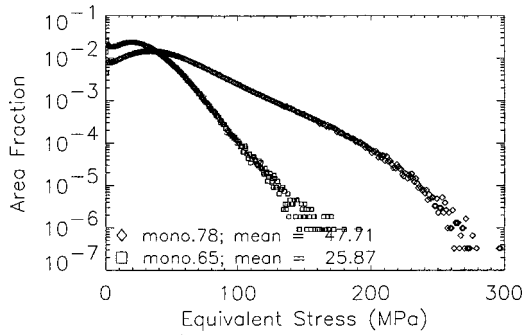


FIG. 5. Equivalent stress difference distributions for  $\gamma=0.65$  and  $\gamma=0.78$  monodisperse granular material.

points) are used in the statistics, resulting in a gentle bend in the data rather than a sharp transition on account of this smoothing. The effect of lowering the initial plastic yield strength to promote plastic deformation is explored later.

The principal stress difference is roughly bounded by the equivalent stress. The von Mises yield criterion is  $3J_2 - Y^2 = 0$ . The relationship between the difference in principal stress and  $J_2$  is given by

$$\Delta\sigma = 2\sqrt{J_2 - \frac{3}{4}s_{33}^2}. \quad (6)$$

From the above equation it is easily seen that the difference in principal stress is bounded,  $\Delta\sigma \leq 2\sqrt{3J_2}/\sqrt{3}$ , where  $\sqrt{3J_2}$  is the equivalent stress. Consequently, the difference in principal stress distribution will reflect that of the equivalent stress. From Fig. 5, the difference in principal stress  $\Delta\sigma \leq 2 \times 300/\sqrt{3} = 346$  MPa, in general agreement with Fig. 4. The data used in Fig. 4 are from material-point stress tensor eigenvalues interpolated directly to computational cells, whereas the data used in Fig. 5 are calculated from the computational cell stress tensors (material-point stress tensors interpolated to computational cells). The former is a sharper representation of particle principal stress differences, and values greater than 346 in Fig. 4 indicate plastic-strain hardening. Note that yielding is not evident for  $\gamma=0.65$  in either Figs. 4 or 5.

Experimentally, the average tangential traction required to shear same-sized spherical glass beads under constant confining pressure and with constant velocity is easily measured and is found to be approximately constant. By comparison, pressure transducer measurements of normal stresses over areas commensurable with grain diameters show that the stresses fluctuate dramatically when force chains contact the transducer. The distribution in time appears to have a more or less exponential tail depending on the number of beads over which the boundary traction is measured. It is postulated that there is a correlation length and once the measurement area is sufficiently large the correlations are washed out and the tail in the distribution boundary traction is exponential [15].

In [16,17], a similar, two-dimensional, experimental study is undertaken. A weakly polydisperse mixture (2500 small disks and 400 22% larger diameter disks) is sheared under constant volume at constant velocity. The disks are photoelastic and allow an estimate of particle contact forces to be made during the deformation. A steady transition in the dis-

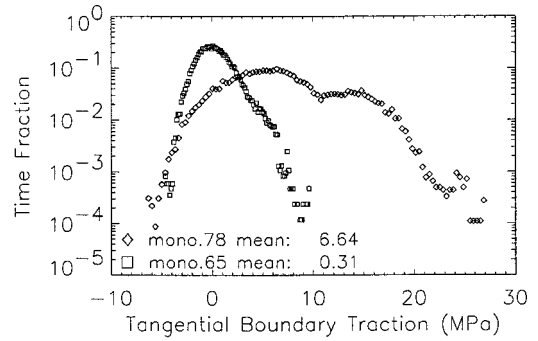


FIG. 6. Tangential boundary traction distributions for  $\gamma=0.65$  and  $\gamma=0.78$  monodisperse granular material.

tribution of particle forces is found. Below the critical packing fraction ( $\gamma \approx 0.78$ ), the distribution is found to be a power law, near the transition exponential, and above it Gaussian. Boundary traction measurements are not made, but are expected to be similar.

One can compare boundary tractions in the constant volume shear simulations with the above measurements. Both normal (confining) and tangential (shearing) tractions are generated during shear. A histogram of the simulated shear tractions for both packing fractions is shown in Fig. 6. Note that negative values of the shearing traction can be recorded when grains affixed to the boundary propagate release waves following collisions or when the force chains buckle. Here the statistics are not nearly as good (data comprised of approximately 60 000 points) as for spatially varying quantities (data comprised of approximately 3 000 000 points) and it is difficult to determine if the histograms have exponential or Gaussian tails, but substantial differences are found between the two packing fractions. Initial transients are discarded as for the stress histograms. The broad distribution in Fig. 6 for  $\gamma=0.78$  is identified, upon further analysis, as the superposition of two narrower distributions. The one with higher mean value corresponds to the occurrence of stress chain banding, and with lower mean value to its absence.

The confining traction histograms are similar, with mean values  $-20.43$  MPa for  $\gamma=0.78$  and  $-3.84$  MPa for  $\gamma=0.65$ . We use the sign convention that stress is positive in tension; therefore, negative normal traction represents a confining boundary pressure. The ratio of the average shear traction to the average confining pressure measures the resistance of the material to shear, or the ‘‘bulk friction,’’  $\bar{\mu}$ . Recall that for both packing fractions the intergranular coefficient of friction is 0.3. For  $\gamma=0.78$ ,  $\bar{\mu}=0.33$ . However, for  $\gamma=0.65$ ,  $\bar{\mu}=0.08$ , indicating resistance to shear is reduced by the development of localized dilation and shear banding. Not surprisingly, a significant contribution to the bulk friction is the frustration of grain motion and subsequent grain deformation in dense packings. The effect of the intergranular coefficient of friction is investigated more extensively for polydisperse grain distributions in the next section.

## B. The effect of polydispersity

Attention is now focused on the shearing of the polydisperse grain distribution depicted in Fig. 1, which is more like real PBXs. The polydisperse sample has a packing fraction

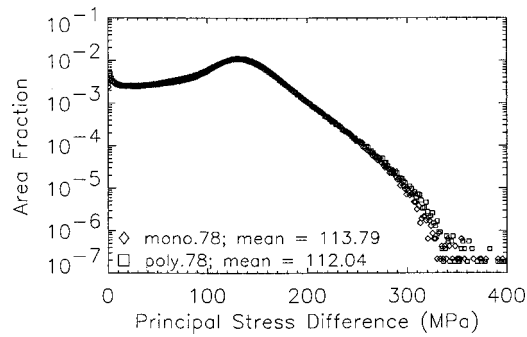


FIG. 7. Principal stress difference distributions for  $\gamma=0.78$  monodisperse and polydisperse granular materials.

$\gamma=0.78$ . Of interest in this section is comparing monodisperse and polydisperse grain size distributions for the same packing fraction, material properties, and intergranular friction coefficient.

Despite the substantial difference in initial geometries, the volume distribution of stress in the “equivalent” polydisperse case is very similar to its monodisperse counterpart. Stress bridging develops similarly, with evolving stress chain networks. However, the initial configuration provides no exceptional resistance to deformation, short-range packing order is never established, and force chain banding does not occur. Only after the initial transients (average shear strain greater than 17%) are data used for statistics, resulting in a data set of nearly 3 500 000 data points from 153 snapshots. The distribution of the difference in principal stresses, Fig. 7, is exponential above the mean and statistically identical to that for the monodisperse case for the same packing fraction. Distributions of equivalent stress are also statistically identical. These similarities suggest that the stress distributions are insensitive to the grain size distribution, and are a general characteristic of the heterogeneous nature of the load carrying mechanism in granular materials.

The effect of polydispersity on the shearing traction can be seen in Fig. 8. In the absence of force chain banding, the distribution has a single maximum. The tails of the distributions are similar in slope for both cases, but no further insight is provided regarding whether they are indicative of an exponential or Gaussian distribution. The computed bulk friction is 0.33 for the monodisperse and 0.48 for the poly-

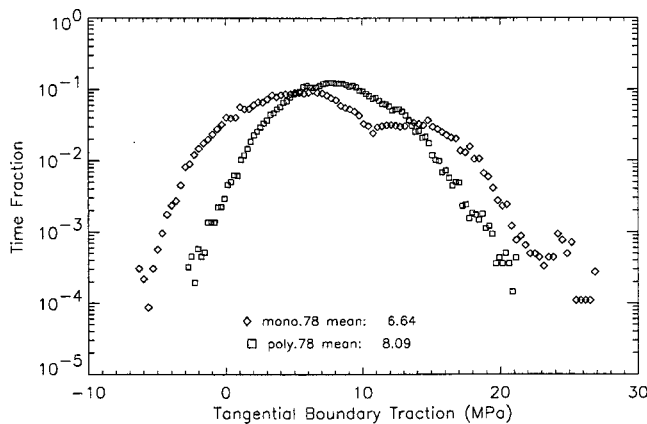


FIG. 8. Tangential boundary traction distributions for  $\gamma=0.78$  monodisperse and polydisperse granular materials.

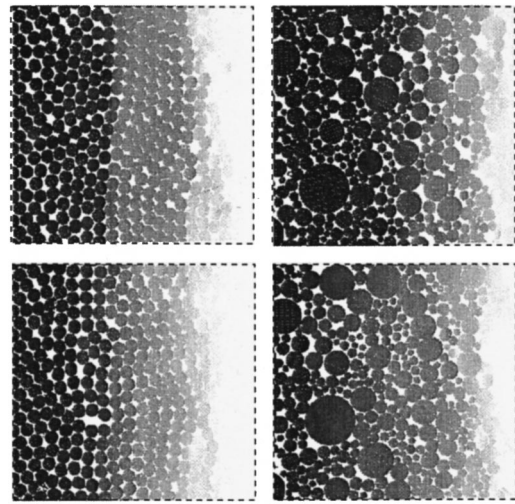


FIG. 9. Normalized displacement magnitudes between grain configurations at 136% and 138% (top) and 248% and 250% (bottom) shear strain for  $\gamma=0.78$  monodisperse and polydisperse granular materials.

disperse sample. The monodisperse sample is easier to shear, in this sense, even though there are larger fluctuations in the boundary tractions due to stress chain banding.

Slip systems develop in the monodisperse case that are not present in the polydisperse one. Incremental displacements between successive snapshots are depicted in Fig. 9 for 138% and 250% shear strain. Black corresponds to no motion between snapshots and white to the maximum. Groups of grains often slide past each other as typified by the left frames of Fig. 9, where the sharp gradients in shading indicate slip lines. The additional frustration caused by the distribution of grain sizes in the polydisperse case prevents slip lines from developing. Instead a more uniform deformation develops, as typified by the right frames, and the bulk friction is higher. Another measure of the system’s resistance to shear is the average power required, which is proportional to the average shear traction. The polydisperse case requires 22% more power to shear.

### C. The effect of friction

Attention is now focused on the polydisperse grain distribution. Of interest in this section are comparisons of simulations with different intergranular friction coefficients and the same grain size distribution, packing fraction, and material properties.

The effect of varying the intergranular coefficient of friction is investigated in simulations for coefficients of friction ranging from 0.0 to 0.5. After discarding initial transients, deformation to 83% shear strain results in 33 snapshots and approximately 700 000 data points. Histograms of equivalent stress for the three coefficients of friction are depicted in Fig. 10. Increasing the coefficient of friction results in larger stresses and additional plastic yielding. A histogram of the difference in principal stress is similar.

Increasing the intergranular coefficient of friction serves to shift boundary traction distributions toward larger tractions with less variation, as illustrated in Fig. 11. Bulk frictions of 0.28, 0.37, and 0.62 are found for coefficients of friction equal to 0.0, 0.3, and 0.5, respectively. The average

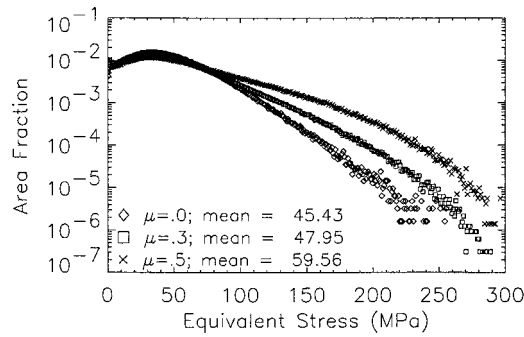


FIG. 10. Equivalent stress distributions for  $\gamma=0.78$  polydisperse granular material as a function of the intergranular coefficient of friction.

power required is 54% and 230% greater, for coefficients of friction 0.3 and 0.5, respectively, than the zero coefficient of friction case. The effect is probably nonlinear and appears to be equally as important as packing fraction.

#### D. The effect of plasticity

Of interest in this section are comparisons of simulations with different material properties, and the same grain size distribution, packing fraction, and intergranular friction coefficient. Here a single material parameter, the plastic yield strength, is varied to promote plastic deformation. Simulations are performed on the polydisperse sample at  $\gamma=0.78$ .

Figure 12 shows the effect on the equivalent stress of reducing the yield strength by one-half to 150 MPa. The simulation is continued to 83% shear strain. The reduction in yield strength does not lead to an obvious increase in plastic deformation. The result seems counterintuitive when considering a homogeneous material where reducing the yield strength should serve to cause more material to yield and make yielded states much more probable. This is not the case for granular materials. The essential feature is that the granular material carries shear by a constantly evolving network of force chains. It is only within the force chains that stresses are high enough to cause yielding. Once a grain is no longer part of a force chain, it unloads elastically. Plastically yielding states are localized to grain contacts in force chains and are uncommon.

The variance of the stress distributions is reduced with reduced yield strength as seen for the equivalent stress in

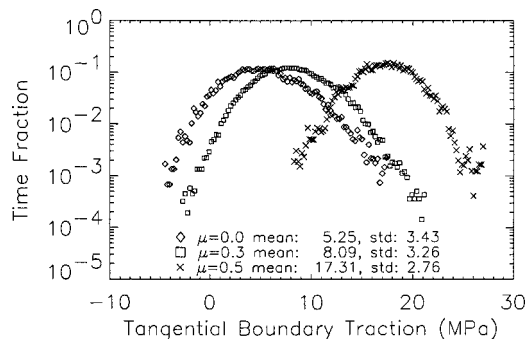


FIG. 11. Tangential boundary traction distributions for  $\gamma=0.78$  polydisperse granular material as a function of the intergranular coefficient of friction.

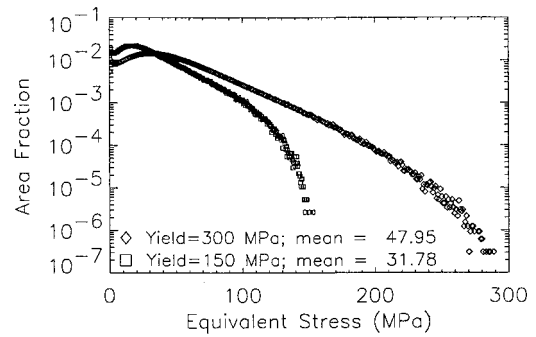


FIG. 12. Equivalent stress distribution for  $\gamma=0.78$  polydisperse granular material as a function of initial plastic yield strength.

Fig. 12. Consequently the spatial distribution of stress is more homogeneous for the lower yield strength case. This can also be seen in Fig. 13, where force chains are compared at 83% shear strain. The plots are of the difference in principal stress, created as described for Figs. 2 and 3. When the yield strength is lower, grains in force chains necessarily carry less force before they begin to yield. (Note the difference in color bar scales for the two different yield strengths in Fig. 12.) For the same applied load, more extensive plastic deformation in the lower yield case results in a denser network of force chains (more lighter areas in the figure) as more grains are brought into contact. The loading is carried more homogeneously in the sense that more grains are involved in the force chain network and the force chains carry lower stresses. Interestingly, ignoring the color bar scales, the ratio of force chain stress to the “background” stress is largely unaffected, indicating a similarity in relative force chain strength.

Decreasing the initial yield strength serves to shift the normal boundary traction distribution toward smaller magnitude tractions with less variation, as illustrated in Fig. 14. The normal boundary traction is calculated as negative in compression consistent with the definition of the stress tensor. The shearing traction distribution has less variation, but the mean is largely unaffected. A bulk friction of 0.58 is found for an initial yield strength of 150 MPa (for a yield strength of 300 MPa, the bulk friction is 0.37). The average power required is 7% greater for the lower yielding material.

For elastic materials, where the growth of  $J_2$  is unconstrained, the stress state has been found experimentally to

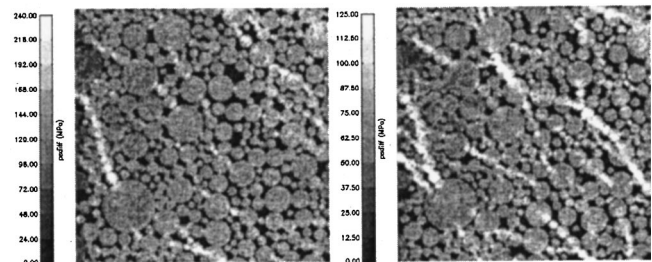


FIG. 13. Force chains at 83% shear for  $\gamma=0.78$  polydisperse granular material as a function of initial plastic yield strength. On the left the initial yield strength is 300 MPa, on the right, 150 MPa. The mean value of the principal stress difference is 112 MPa with a threshold of 212 MPa on the left, and a mean of 59 MPa and a threshold of 116 MPa on the right. Material with values of the principal stress difference above the threshold are white.

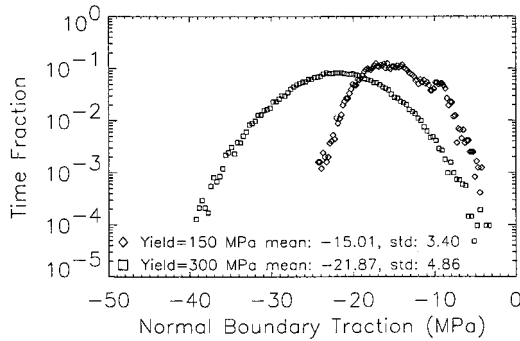


FIG. 14. Normal boundary traction distributions for  $\gamma=0.78$  polydisperse granular material as a function of initial plastic yield strength.

give rise to an exponential spatial distribution of  $\Delta\sigma$  (using photoelasticity [14]). The authors are unaware of any ‘photoelastic-plastic’ materials, but if there were, optical techniques could be used to detect plastic yielding in granular materials.

During large shear, permanent deformation should occur first at grain edges where large contact stresses are experienced. However, little apparent deformation of the grains is observed. Grains deform plastically when participating in strong force chains, but otherwise elastically. Evidently, the transient nature of the force chains results in compression of the grains from different directions and no obvious permanent bulk deformation.

#### E. The effect of grain shape

Of interest in this section is a comparison of simulations with cylindrical and hexagonal grain shapes, and the same grain size distribution, packing fraction, material properties, and intergranular friction coefficient. The initial geometry, with hexagonal cross sections replacing the circular ones, is shown in Fig. 15.

The effect of varying the cross sectional grain shape is investigated by performing a simulation to 83% shear strain. Histograms of equivalent stress for both grain shapes are depicted in Fig. 16. The histograms are similar, although for hexagonal grain shapes the stresses are systematically larger. A histogram of the difference in principal stress is similar. As might be expected, granular contact between grains with corners results in the generation of larger stresses.

The nominal value of 0.3 for the intergranular Coulomb friction coefficient results in a bulk friction for the hexagonal cross sections of 0.52, compared with 0.48 for circular cross sections. The average power required is 50% greater for hex-

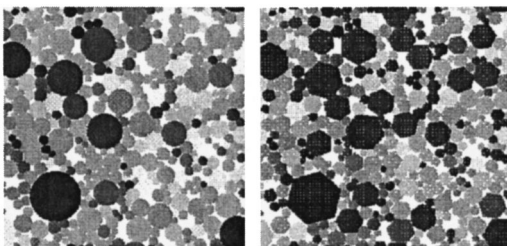


FIG. 15. Initial configurations for  $\gamma=0.78$  polydisperse granular material with cylindrical and hexagonal cross sections.

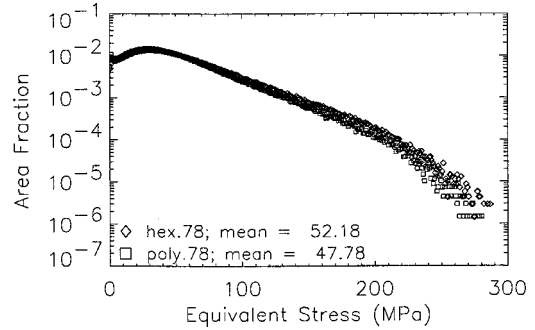


FIG. 16. Equivalent stress distribution for  $\gamma=0.78$  polydisperse granular material as a function of initial cylinder cross-section shape.

agonal cross sections. Both measures of resistance to shear indicate that grains with corners are more difficult to shear.

#### IV. CONCLUSIONS

Through micromechanical simulations with deformable grains we have sought to extend our understanding of granular materials to include some of the properties of real materials, including polydispersity, friction, varying grain shape, and plastic deformation. Most of the simulations are for packing fractions close to what has been described as the critical packing fraction,  $\gamma=0.78$ , but one simulation at lower packing fraction,  $\gamma=0.65$ , illustrates some of the changes that can occur when the density is decreased. The most striking feature of all of the simulations, as in experiments and simulations of granular materials reported by others, is the high degree of spatial correlation at each instant and the simultaneous high level of fluctuations in the stress over time. Arguments based on the decorrelation of stress chains in time allow us to assemble the data from the computed response of granular materials to applied shearing strain into a probability density function for the volume distribution of the difference in the principal stress. Exponential distributions of principal stress difference, above the mean, are found in all cases. The form of the stress distribution persists under a variety of material parameters, grain geometries, and packing fractions, indicating that these distributions are characteristic of the heterogeneous nature of granular media where loads are carried by a small fraction of the material in force chains. If further studies should confirm the results of these simulations, we speculate that descriptions of the bulk properties of granular materials might be based on knowledge of the probability distribution function for the stress.

Because there are few materials for which the stress distribution in the volume can be measured directly, we have explored the possibility that measurements of the statistics of surface traction can be related to the volume stress distribution. The results of the simulations are ambiguous, as are those from experiments, on whether the surface traction distribution is Gaussian or exponential in form. In the case of the simulations, one obvious difficulty is that the data sets from which the distributions must be inferred are much smaller for the boundary than those for the volume.

Although distributions of stress are similar in character in all cases, the ease with which granular material can be

sheared depends strongly on all of the parameters. The bulk friction coefficient, as measured by the ratio of tangential to normal components of traction on the boundary, is always higher than the intergranular Coulomb friction coefficient when the packing fraction is near critical,  $\gamma=0.78$ , but is smaller when  $\gamma=0.65$ . We find that monodisperse samples are easier to shear than polydisperse samples. Slip systems develop in the monodisperse case that appear to be frustrated by the grain size distribution for polydisperse samples. As might be anticipated, increasing the intergranular Coulomb friction coefficient results in larger stresses and additional plastic yielding, although the relationship appears to be nonlinear. Changing the grain shape from disks to hexagons also shifts stress distributions to higher values, even though the intergranular friction coefficient is the same.

A new phenomenon, force chain banding, is observed in the monodisperse sample at the critical packing fraction and has been shown to correspond to recrystallization of the material. Configurations with regions of grains in a regular hexagonal packing have larger tangential boundary tractions on average, resulting in a higher bulk friction coefficient for these states. For the polydisperse sample, crystalline packing is not possible and no force chain banding is observed.

Also not previously observed is the effect of plastic yielding. Surprisingly, yielded states are relatively rare even when the yield strength of the grains is reduced in dense packings. Plastically yielded states are localized to grain contacts

within force chains and grains unload elastically when not part of a chain. Under shear, force chains are constantly evolving and are short lived; however, there tend to be more chains at any given instant in the lower-yield material. The higher chain density reflects a more uniform stress distribution, i.e., the width of the distribution is decreased.

Our direct numerical simulations incorporate the best available information regarding constitutive behavior of each grain, which allows us to simulate specific materials and to make direct connections to experiments, and even to extend our investigations beyond current experimental capabilities. Most experimental work for which the deformation is characterized on the scale of the grains is on cylindrical or spherical particles of uniform size. Far less experimental data exist for other shapes and size distributions. In part this is due to the desirability of using photoelasticity to obtain experimental information, and the difficulty in obtaining prepared photoelastic grains in other shapes. The use of photoelastic materials also limits the range of material properties and interfacial friction that can be investigated. Direct numerical simulations as reported here suffer no such limitations.

#### ACKNOWLEDGMENT

This research is supported by the U.S. Department of Energy, under Contract No. W-7405-ENG-36.

- 
- [1] H. Jaeger, S. Nagel, and R. Behringer, *Rev. Mod. Phys.* **68**, 1259 (1996).
  - [2] A. Mehta and G. C. Barker, *Rep. Prog. Phys.* **57**, 383 (1994).
  - [3] P. G. de Gennes, *Physica A* **261**, 267 (1998).
  - [4] S. Coppersmith *et al.*, *Phys. Rev. E* **53**, 4673 (1996).
  - [5] A. Drescher and G. de Josselin de Jong, *J. Mech. Phys. Solids* **20**, 337 (1972).
  - [6] T. Travers *et al.*, *J. Phys. (France)* **49**, 939 (1988).
  - [7] F. Radjai, M. Jean, J.-J. Moreau, and S. Roux, *Phys. Rev. Lett.* **77**, 274 (1996).
  - [8] C. Campbell, *Acta Mech.* **104**, 65 (1994).
  - [9] L. P. Kadanoff, *Rev. Mod. Phys.* **71**, 435 (1999).
  - [10] D. Benson, *Modell. Simul. Mater. Sci. Eng.* **2**, 535 (1994).
  - [11] S. Bardenhagen, J. Brackbill, and D. Sulsky (unpublished).
  - [12] C. Liu *et al.*, *Science* **269**, 513 (1995).
  - [13] D. M. Mueth, H. M. Jaeger, and S. R. Nagel, *Phys. Rev. E* **57**, 3164 (1999).
  - [14] G. W. Baxter, in *Powders and Grains 97* (Balkema, Rotterdam, 1997), pp. 345–348.
  - [15] B. Miller, C. O'Hern, and R. P. Behringer, *Phys. Rev. Lett.* **77**, 3110 (1996).
  - [16] D. W. Howell, R. P. Behringer, and C. T. Veje, *Chaos* **9**, 559 (1999).
  - [17] C. T. Veje, D. W. Howell, and R. P. Behringer, *Phys. Rev. E* **59**, 739 (1999).
  - [18] O. Schwarz, Y. Horie, and M. Shearer, *Phys. Rev. E* **57**, 2053 (1998).
  - [19] J. K. Morgan and M. S. Boettcher, *J. Geophys. Res., [Solid Earth]* **104**, 2703 (1999).
  - [20] J. K. Morgan, *J. Geophys. Res., [Solid Earth]* **104**, 2721 (1999).
  - [21] D. Sulsky, Z. Chen, and H. L. Schreyer, *Comput. Methods Appl. Mech. Eng.* **118**, 179 (1994).
  - [22] D. Sulsky, S.-J. Zhou, and H. L. Schreyer, *Comput. Phys. Commun.* **87**, 236 (1995).
  - [23] D. Sulsky and H. L. Schreyer, *Comput. Methods Appl. Mech. Eng.* **139**, 409 (1996).
  - [24] P. Cundall and O. D. L. Strack, *Geotechnique* **29**, 47 (1979).
  - [25] P. A. Cundall, *Int. J. Rock Mech. Min. Sci. Geomech. Abstr.* **25**, 107 (1988).
  - [26] S. Bardenhagen, J. Brackbill, and D. Sulsky, *Comput. Methods Appl. Mech. Eng.* **187**, 529 (2000).
  - [27] J. K. A. Amuzu, B. J. Briscoe, and M. M. Chaudhri, *J. Phys. D* **9**, 133 (1976).
  - [28] C. B. Skidmore, D. S. Phillips, and N. B. Crane, *Microscope* **45**, 127 (1997).